Acta Crystallographica Section B
Structural Science
ISSN 0108-7681

Framework 'interstitial' oxygen in $La_{10}(GeO_4)_5(GeO_5)O_2$ apatite electrolyte

Stevin S. Pramana,[a] Wim T. Klooster[a,b] and T. J. White[a]*

[a]Nanyang Technological University, School of Materials Science and Engineering, 50 Nanyang Avenue, 639798 Singapore, and [b]Institute of Materials Research and Engineering, 3 Research Link, 117602 Singapore

Correspondence e-mail: tjwhite@ntu.edu.sg

Received 19 April 2007
Accepted 17 May 2007

Oxygen conduction at low temperatures in apatites make these materials potentially useful as electrolytes in solid-oxide fuel cells, but our understanding of the defect structures enabling ion migration is incomplete. While conduction along [001] channels is dominant, considerable inter-tunnel mobility has been recognized. Using neutron powder diffraction of stoichiometric '$La_{10}(GeO_4)_6O_3$', it has been shown that this compound is more correctly described as an $La_{10}(GeO_4)_5(GeO_5)O_2$ apatite, in which high concentrations of interstitial oxygen reside within the channel walls. It is suggested that these framework interstitial O atoms provide a reservoir of ions that can migrate into the conducting channels of apatite, *via* a mechanism of inter-tunnel oxygen diffusion that transiently converts GeO_4 tetrahedra to GeO_5 distorted trigonal bipyramids. This structural modification is consistent with known crystal chemistry and may occur generally in oxide apatites.

1. Introduction

Apatite ceramics accommodate diverse chemistries suitable for the remediation of radioactive waste (Ohnuki *et al.*, 2004), catalysis (Smahi *et al.*, 2003), reconstructive medicine (Harrison *et al.*, 2004) and non-toxic pigments (Karpov *et al.*, 2003). They are also candidate low-temperature (773–1023 K) solid-oxide fuel cell (SOFC) electrolytes (Nakayama *et al.*, 1995; Slater & Sansom, 2003; Slater *et al.*, 2004), the most promising to date being nonstoichiometric lanthanum silicates and germanates (Abram *et al.*, 2005; Islam *et al.*, 2003). The crystal chemical formula for hexagonal $P6_3/m$ apatites is $[A^{\rm I}_4][A^{\rm II}_6][(BO_4)_6][X]_2$, where A and B are larger and smaller cations, respectively, and X is an anion or oxy-anion. The structure has zeolitic character being constructed of an $A^{\rm I}_4(BO_4)_6$ framework that circumscribes [001] channels whose size adjusts to accommodate the $A^{\rm II}_6X_2$ component (Povarennykh, 1972; see Fig. 1). The diameter of this conduit is controlled by (001) twisting of the triangular faces of $A^{\rm I}O_6$ metaprisms through an angle ϕ such that larger rotations constrict the tunnel when either the size or abundance of the $A^{\rm II}$ and X atoms decreases, in a process that leaves the BO_4 tetrahedron essentially undistorted. While $5 \leq \phi \leq 24^\circ$ is commonly encountered (White & ZhiLi, 2003; White *et al.*, 2005), larger twist angles [as in $Ca_{10}(VO_4)_6F_2$ for example; Baikie *et al.*, 2007] require the tetrahedron to rotate about $[100]_{\rm hex}$ to furnish acceptable bond-valence sums and in so doing, the lattice symmetry is reduced from hexagonal to triclinic.

In apatite electrolytes it has been a general presumption – based on conductivity measurements (Nakayama *et al.*, 1995;

Slater & Sansom, 2003), crystallographic investigations (Nakayama *et al.*, 1995; Slater *et al.*, 2004) and semi-empirical simulations (Tolchard *et al.*, 2003) – that mobile interstitial oxygen appears exclusively in the [001] tunnel close to the *X* anion position. León-Reina *et al.* (2003) showed that $La_{10-x}(GeO_4)_6O_{3-1.5x}$ adopts $P6_3/m$ symmetry across the compositional range $9.52 \leq 10-x \leq 9.60$ with a phase transformation to triclinic $P\bar{1}$ at higher lanthanum contents ($9.66 \leq 10-x \leq 9.75$). In a subsequent investigation of $La_{9.55}(SiO_4)_6O_{2.32}$ and $La_{9.60}(GeO_4)_6O_{2.40}$ using neutron diffraction (León-Reina *et al.*, 2004), excess scattering in the tunnels was attributed to crystallographic sites containing interstitial oxygen at rather small occupancy factors (< 0.05), in agreement with atomistic simulation (Tolchard *et al.*, 2003). A recent comparison of the anion sublattices for a range of germanate and silicate analogues suggests that low concentrations of interstitial oxygen reside nearer the framework walls of the former, but are forced towards the tunnel centre in the latter (León-Reina *et al.*, 2004, 2006; León-Reina, Losilla, Martinez-Lara, Bruque *et al.*, 2005; León-Reina, Losilla, Martinez-Lara *et al.*, 2005; Tolchard *et al.*, 2003, 2005). For stoichiometric $La_8Sr_2(SiO_4)_6O_2$, oxygen-ion migration through the tunnel by a 'vacancy' mechanism was calculated to be energetically favourable, while in nonstoichiometric $La_{9.33}(SiO_4)_6O_2$ an 'interstitial' movement was preferred (Tolchard *et al.*, 2003). Indeed, both conductivity measurements and theoretical studies have focused almost solely on intra-tunnel oxygen transport. However, Nakayama & Higuchi (2001) reported significant oxygen-ion conduction perpendicular to the channels in single crystals of $Pr_{9.33}(SiO_4)_6O_2$, $Nd_{9.33}(SiO_4)_6O_2$ and $Sm_{9.33}(SiO_4)_6O_2$. In this paper we describe the crystal structure of stoichiometric $La_{10}(GeO_4)_5(GeO_5)O_2$ and the direct determination of interstitial oxygen at high concentrations within the walls of the apatite framework, rather than at dilute tunnel sites. This data has allowed the development of a mechanism of inter-tunnel oxygen passage, in addition to the commonly accepted intra-tunnel migration.

Table 1
Experimental details.

Crystal data	
Chemical formula	$La_{10}Ge_6O_{27}$
M_r	2256.70
Cell setting, space group	Triclinic, $P\bar{1}$
Temperature (K)	300
a, b, c (Å)	9.9346 (7), 9.9132 (7), 7.3021 (5)
α, β, γ (°)	90.960 (5), 88.079 (5), 120.890 (4)
V (Å^3)	616.8 (1)
Z	1
D_x (Mg m^{-3})	6.076
Radiation type	Neutron
Specimen form	Cylinder
Data collection	
Diffractometer	Local
Data collection method	Specimen mounting: vanadium can with He exchange gas; reflection; scan method: fixed
2θ (°)	$2\theta_{min} = 9$, $2\theta_{max} = 150$
Refinement	
R factors and goodness-of-fit	$R_p = 0.039$, $R_{wp} = 0.050$, $R_{exp} = 0.070$, $R_B = 0.014$, $S = 0.72$
Wavelength of incident radiation (Å)	1.8834
Excluded regions	0.027–8.97° unreliable due to background
No. of parameters	129
Weighting scheme	Based on measured s.u.'s
$(\Delta/\sigma)_{max}$	<0.0001

Computer programs used: Shimadzu XRD 6000; *TOPAS* (Bruker, 2005), *ATOMS* (Dowty, 2004), *GFOURIER* (Gonzales-Platas & Rodriguez-Carvajal, 2006).

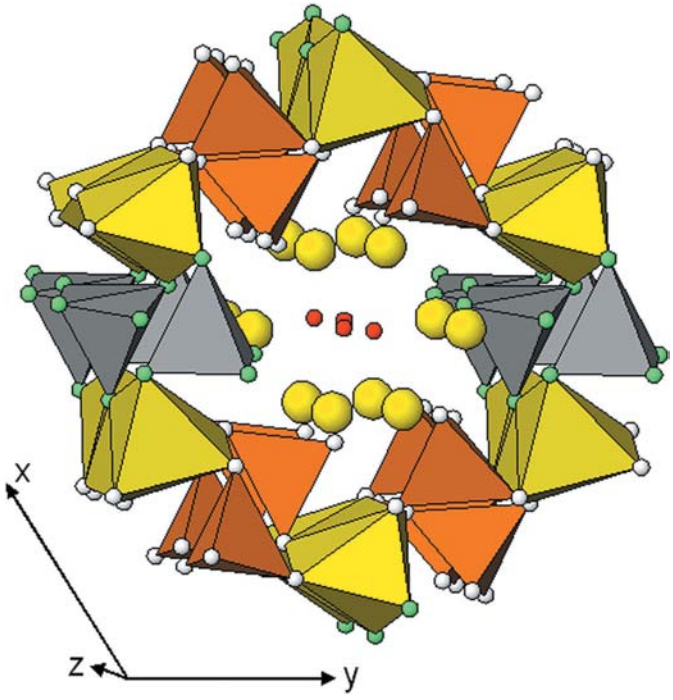

Figure 1
An [001] polyhedral representation of triclinic $La_{10}(GeO_4)_5(GeO_5)O_2$ apatite emphasizing the average structure in which face-sharing LaO_6 metaprisms (yellow) are corner-connected to GeO_4 tetrahedra (brown) and GeO_5 trigonal bipyramids (grey) to create an adaptable framework. The [001] channel contains La3, La4, La5 (yellow) and O13 (red). Metaprism twisting adjusts the channel diameter as a function of stoichiometry.

2. Experimental

$La_{10}(GeO_4)_5(GeO_5)O_2$ was synthesized by solid-state reaction.

$$5La_2O_3 + 6GeO_2 \rightarrow La_{10}(GeO_4)_5(GeO_5)O_2 \qquad (1)$$

La_2O_3 (BDH, 99.5%) and GeO_2 (Alfa Aesar, 99.999%) were dehydrated for 4 h at 1273 and 873 K, respectively, after which stoichiometric amounts were manually ground in an agate mortar and pestle and calcined at 1373 K for 16 h. These powders were reground and sintered at 1573 K for another 16 h in a platinum crucible.

Neutron powder diffraction data were collected on the high-resolution powder diffractometer (HRPD) at the High

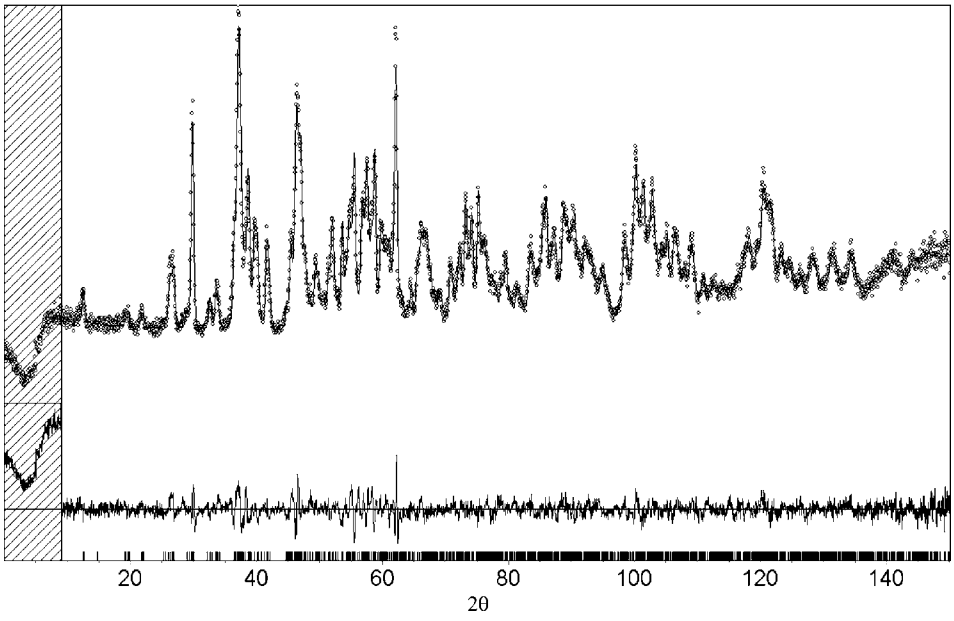

Figure 2
Rietveld plot of the neutron diffraction data of $La_{10}(GeO_4)_5(GeO_5)O_2$ collected at room temperature. The observed intensity data are shown by dots, with the solid line representing the calculated intensity. Differences between observed and calculated intensities are plotted beneath. Vertical markers indicate the Bragg reflections.

Flux Australian Reactor (HIFAR) operated by the Australian Nuclear Science and Technology Organization (ANSTO). Approximately 15 g of the apatite was loaded into a 12 mm diameter vanadium can that was rotated during data collection. The diffraction data were accumulated at ambient temperature using a neutron wavelength of 1.8834 (1) Å from 0.027 to 150.027° 2θ in 0.05° steps.

The crystal structure of $La_{10}(GeO_4)_5(GeO_5)O_2$ was refined by Rietveld analysis (Rietveld, 1969) using data from 9 to 150° in 2θ and a pseudo-Voigt peak-shape profile as implemented in *TOPAS* (Bruker, 2005). Difference-Fourier maps were generated using *GFOURIER* (Gonzales-Platas & Rodriguez-Carvajal, 2006) embedded in *FULLPROF* (Rodriguez-Carvajal, 1990). The starting model used the atomic positions of $La_{10-x}(GeO_4)_6O_{3-1.5x}$ ($9.66 \leq 10-x \leq 9.75$) for $P\bar{1}$ (León-Reina *et al.*, 2003). For each data set, a five-coefficient Chebychev polynomial and $1/x$ background, a zero error, unit-cell parameters, scale factors and crystal size were refined sequentially. Neutron scattering lengths of 0.824, 0.81929 and 0.5803×10^{-12} cm were used for La, Ge and O, respectively (Sears, 1993). The cation positions were refined first, followed by the oxygen positions. The Ge3 tetrahedron was modelled with disordered positions. Isotropic displacement parameters for all atoms were refined with La1/La2; La3/La4/La5; all O except O13 (the tunnel anion) constrained to have the same value. A total of 106 independent variables were refined. The Rietveld plot is given in Fig. 2.[1]

[1] Supplementary data for this paper are available from the IUCr electronic archives (Reference: LM5010). Services for accessing these data are described at the back of the journal.

3. Results and discussion

It is evident that $La_{10}(GeO_4)_6O_3$ contains an extra anion compared with the nominal $A_{10}(BO_4)_6X_2$ formulation and in terms of descriptive crystallography, this oxygen might be located within the channels (the conventional view) or through conversion of the BO_4 tetrahedron to a BO_5 polyhedron [as in $Ba_{10}(ReO_5)_6Cl_2$ for example; Besse *et al.*, 1979]. Rietveld analysis of neutron powder diffraction data for $La_{10}Ge_6O_{27}$ converged successfully in the lower-symmetry $P\bar{1}$ rather than $P6_3/m$, as would be expected if the framework was large relative to the tunnel contents. Fourier difference (001) sections through the tunnel confirmed that two central oxygens (the X sites) sufficiently accounted for all the scattering in this region. Similar mapping of the framework clearly revealed the remaining oxygen was located statistically at 'interstitial' positions between the $Ge3O_4$ tetrahedra with an average occupancy of 0.5 (Fig. 3). In order to obtain reasonable Ge—O bond distances, the Ge3 atom was disordered over a nearby Ge3a site. The final crystallographic parameters distribute the interstitial oxygen O14 over 2(i) Wyckoff positions at the fractional coordinates ±[0.028 (4), 0.477 (4), 0.511 (5)], leading to a more appropriate description of this apatite as

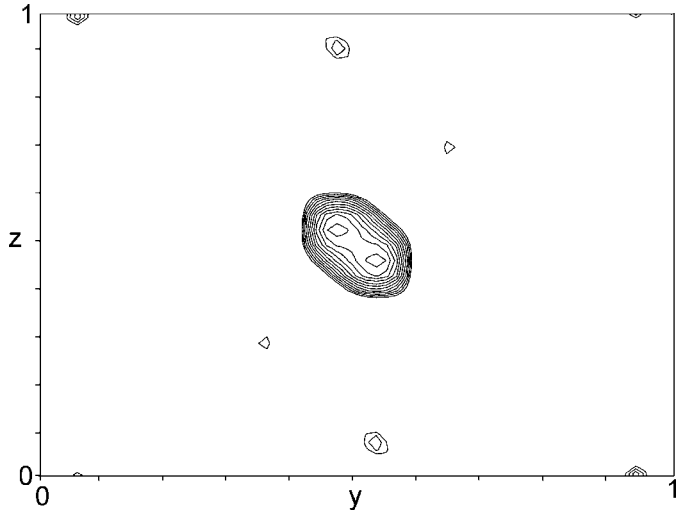

Figure 3
Difference-density Fourier map at $x = 0$ for $La_{10}(GeO_4)_5(GeO_5)O_2$ showing the split oxygen interstitial O14 at ± [0.028 (4), 0.477 (4), 0.511 (5)] with an occupancy of 50%.

Table 2
Selected bond distances (Å) for $La_{10}(GeO_4)_5(GeO_5)O_2$.

La1—O3	2.18 (5)	La5—O13	2.24 (2)
La1—O6*a*	2.39 (4)	La5—O7	2.42 (2)
La1—O3*a*	2.45 (4)	La5—O12*a*	2.43 (4)
La1—O2	2.50 (2)	La5—O10	2.47 (2)
La1—O1	2.55 (2)	La5—O9	2.62 (5)
La1—O9	2.57 (3)	La5—O12	2.69 (5)
La1—O5	2.57 (2)	La5—O4	2.71 (2)
La1—O6	2.60 (4)	La5—O8	2.74 (2)
La1—O4	2.63 (2)	La5—O2	2.79 (2)
La1—O7	2.66 (2)	La5—O9*a*	2.81 (5)
La1—O9*a*	2.76 (3)	Average	2.59
Average 2.53			
		Ge1—O1	1.73 (3)
La2—O6*a*	2.11 (4)	Ge1—O4	1.86 (2)
La2—O14	2.38 (3)	Ge1—O7	1.80 (1)
La2—O3	2.49 (4)	Ge1—O10	1.76 (2)
La2—O2	2.51 (2)	Average	1.79
La2—O4	2.53 (2)		
La2—O1	2.55 (2)	Ge2—O2	1.68 (2)
La2—O6	2.63 (4)	Ge2—O5	1.79 (2)
La2—O11	2.63 (3)	Ge2—O8	1.79 (2)
La2—O5	2.66 (2)	Ge2—O11	1.81 (2)
La2—O3*a*	2.73 (4)	Average	1.77
La2—O14	2.83 (4)		
Average	2.55	Ge3—O3	1.88 (4)
		Ge3—O6	1.78 (5)
La3—O13	2.44 (3)	Ge3—O9	1.79 (5)
La3—O12*a*	2.47 (3)	Ge3—O12	1.97 (5)
La3—O8	2.47 (2)	Ge3—O14	2.01 (4)
La3—O10	2.49 (2)	Average	1.89
La3—O5	2.50 (2)		
La3—O11	2.54 (2)	Ge3*a*—O3*a*	1.85 (3)
La3—O7	2.77 (2)	Ge3*a*—O6*a*	1.60 (3)
La3—O3	2.79 (5)	Ge3*a*—O9*a*	2.01 (4)
La3—O3*a*	2.92 (4)	Ge3*a*—O12*a*	2.21 (5)
Average	2.60	Ge3*a*—O14	1.88 (4)
		Average	1.91
La4—O9*a*	2.22 (4)		
La4—O13	2.27 (3)	Split sites	
La4—O6	2.36 (5)	Ge3—Ge3*a*	0.51 (4)
La4—O12	2.36 (4)	O3—O3*a*	0.54 (5)
La4—O1	2.51 (2)	O6—O6*a*	0.62 (4)
La4—O8	2.53 (2)	O9—O9*a*	0.44 (4)
La4—O11	2.56 (2)	O12—O12*a*	0.87 (5)
La4—O12*a*	2.63 (3)		
La4—O9	2.64 (4)		
La4—O14	2.79 (4)		
La4—O6*a*	2.80 (5)		
Average	2.52		

$La_{10}(GeO_4)_5(GeO_5)O_2$, rather than $La_{10}(GeO_4)_6O_3$, since the latter implies the extra oxygen is located in the channel (Table 1). Lowering the symmetry to *P*1 did not significantly improve the residual factors, while attempts to fit the data to previously reported models containing tunnel oxygen interstitials yielded inferior refinements.

The framework interstitial oxygen being disordered over two symmetry-related sites ~0.90 (9) Å apart promotes cooperative displacements of the Ge3, O3, O6, O9 and O12 atoms that create additional split crystallographic sites all with an occupancy factor of 0.5. This structural model permits the re-analysis of oxygen migration in SOFC apatites. The Ge3 is displaced 0.51 (4) Å towards the face of the tetrahedron to create a Ge3*a* position that bonds with O14 and forms a distorted Ge3*a*O_5 trigonal bipyramid (Fig. 4). While the Ge3—O3, 6, 9, 12, 14 bond lengths range from 1.78 (5) to 2.01 (4) Å, the framework O14 extends the Ge3*a*—O12*a* bond to 2.21 (5) Å, pushing the O12*a* atom 0.87 (5) Å towards the tunnel centre (Table 2). The close approach of the O14 site pairs and the cooperative distortion of the GeO_5 polyhedra facilitate migration across the framework wall by rotation of the polyhedron to satisfy bond-length requirements. During ion migration it is believed that O14 displaces O12/O12*a*, rather than O3/O3*a*, O6/O6*a* or O9/O9*a* which are more strongly bonded to the lanthanum-metaprism framework (La1 and La2; Table 2), in a manner that provides a clear pathway for the oxygen migration along [010].

Tolchard *et al.* (2003) predicted, using semi-empirical methods, that the lowest energy route for vacancy migration in $La_8Sr_2(SiO_4)_6O_2$ was along the tunnel with saddle-points between the O13 tunnel positions. Similarly, for O12*a* to move through the framework and across the tunnel an 'intermediate' position/saddle-point is required at around (0, 0, 0.5) between the statistically occupied O13 sites. The distance between O12*a* – (0, 0, 0.5) is ~2.10 (5) Å. The sinusoidal-like ionic movement in the *b* direction across the channels can be described by the motion ...O12*a*/O12 – O14/O14*a* – O12*a*/O12 – (0, 0, 0.5) – O12*a*/O12... (Fig. 5). In combination with the model of Tolchard *et al.* (2003), this new mechanism explains why ions can be transported both within and between tunnels. The comparatively large displacement parameter for O13 may be caused by anisotropy in thermal motion or even static displacement (Okudera *et al.*, 2005), consistent with intra- and inter-tunnel migration. It can also be postulated that the high concentration of framework 'interstitial' oxygen provides a reservoir of oxygen ions that move to the large tunnels where they more easily migrate through the structure. It is of interest that Kharton *et al.* (2004) in a Mössbauer spectroscopic analysis of $La_{10}Si_5FeO_{26.5}$ electrolytes reported

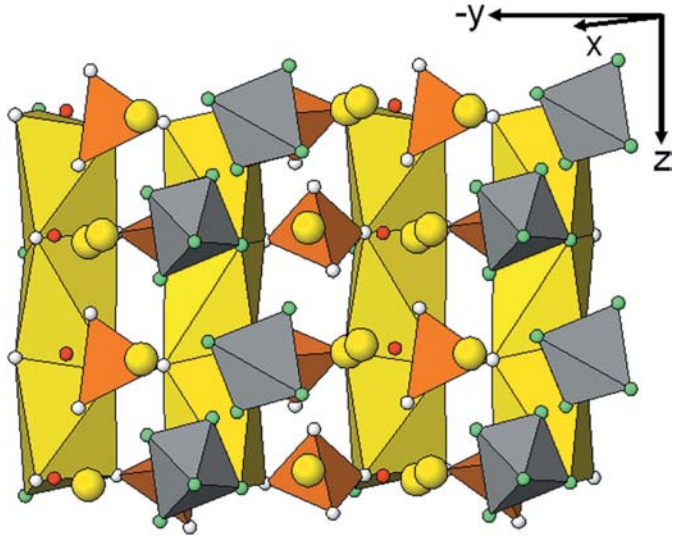

Figure 4
A polyhedral drawing demonstrating the conversion of GeO_4 tetrahedra (brown) to GeO_5 trigonal bipyramids (grey) through the inclusion of the framework 'interstitial' oxygen O14 at occupancy 0.5. The LaO_6 metaprisms (yellow) are obviously distorted. The O13 tunnel oxygen is shown in red.

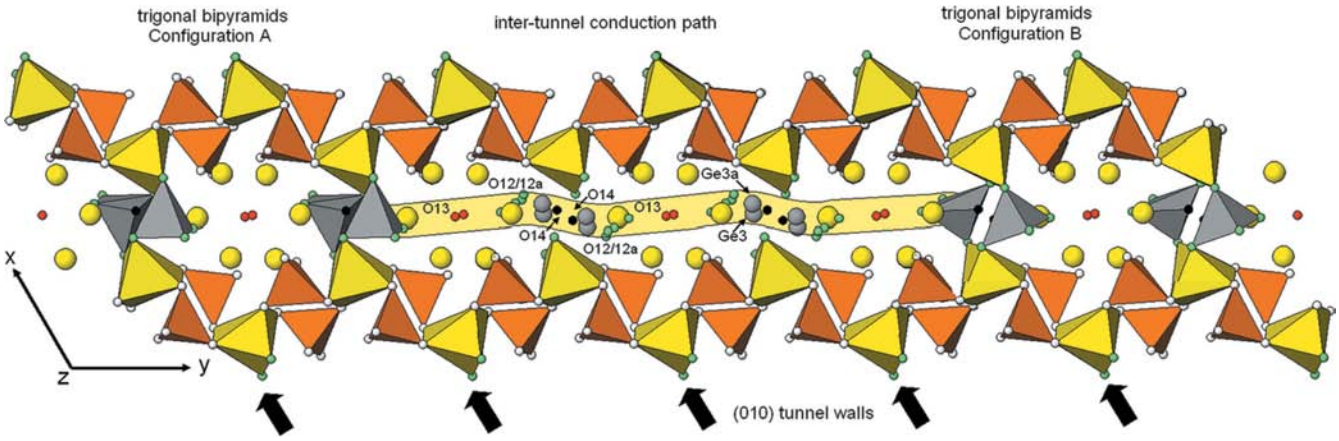

Figure 5
Proposed inter-tunnel migration path for oxygen in $La_{10}(GeO_4)_5(GeO_5)O_2$. The two configurations (*A* and *B*) of the GeO_5 trigonal bipyramids (grey) are emphasized on the left and right, where the complete framework is shown. In the central portion of the drawing all the statistically occupied germanium (Ge3/Ge3*a*) and oxygen (O12, O13, O14) sites are included to demonstrate the feasibility of creating an ion migration pathway (yellow band). Note that O12/O12*a* is displaced towards the centre of the tunnel with ion movement proposed to take place through a saddle-point (0, 0, 0.5) between the O13 [0.004 (2), 0.020 (3), 0.237 (3)] atoms.

partial conversion of the tetrahedra to five-coordination for a sample showing the highest oxygen conduction. Further study will be required to validate this ion-migration mechanism and also the role of microstructural defects. In this regard it is noted that at the unit-cell scale the crystallochemical properties of apatites can be surprisingly intricate. It has recently been shown that natural and synthetic apatites form nanometric domains to accommodate local changes in stoichiometry (Dong & White, 2004; Ferraris *et al.*, 2005), although their recognition by high-resolution transmission electron microscopy can be compromised owing to the accumulation of electron beam damage. Such fine features are not readily detected by powder diffraction. Moreover, single value decomposition analysis of Rietveld parameters has shown unreliable convergence of apatite structures during refinement and therefore more sophisticated methods of geometric parameterization and *ab initio* simulation are required (Mercier *et al.*, 2005, 2006). Concerning the present data, the possibility of non-stoichiometry within the La1/La2O_6 metaprisms could not be satisfactorily analysed and should not be discounted.

4. Conclusions

$La_{10}(GeO_4)_5(GeO_5)O_2$ apatite synthesized at 1573 K adopts the $P\bar{1}$ structure. The interstitial oxygen O14 with an occupancy of 0.5 is located at the fractional coordinates $\pm$ [0.028 (4), 0.477 (4), 0.511 (5)], promoting the transformation of a Ge3O_4 tetrahedron to a Ge3*a*O_5 trigonal bipyramid. It is believed that migration of O14 associated with displacement of O12/O12*a* provides a pathway for cooperative inter-tunnel and intra-tunnel ion transport in SOFC apatite electrolytes. Further investigation of analogous oxygen-excess apatites would be helpful in establishing the universality of framework interstitial oxygen and its role in conductivity.

References

Abram, E. J., Kirk, C. A., Sinclair, D. C. & West, A. R. (2005). *Solid State Ion.* **176**, 1941–1947.
Baikie, T., Elcombe, M. M., Mercier, P. H. J., Kim, J. Y., Le Page, Y., Mitchell, L. D., White, T. J. & Whitfield, P. S. (2007). *Acta Cryst.* B**63**, 251–256.
Besse, P. J.-P., Baud, G., Levasseur, G. & Chevalier, R. (1979). *Acta Cryst.* B**35**, 1756–1759.
Bruker (2005). *TOPAS*, Version 3. Bruker AXS Inc., Madison, Wisconsin, USA.
Dong, Z. & White, T. J. (2004). *Acta Cryst.* B**60**, 138–145.
Dowty, E. (2002). *ATOMS*, Version 6.0. Shape Software, 521 Hidden Valley Road, Kingsport, TN 37663, USA.
Ferraris, C., White, T., Plévert, J. & Wegner, R. (2005). *Phys. Chem. Miner.* **32**, 485–492.
Gonzales-Platas, J. & Rodriguez-Carvajal, J. (2006). *GFOURIER*, Version 04.05. Universidad de la Laguna, Tenerife, Spain.
Harrison, J., Melville, A. J., Forsythe, J. S., Muddle, B. C., Trounson, A. O., Gross, K. A. & Mollard, R. (2004). *Biomaterials*, **25**, 4977–4986.
Islam, M. S., Tolchard, J. R. & Slater, P. R. (2003). *Chem. Commun.* pp. 1486–1487.
Karpov, A. S., Nuss, J., Jansen, M., Kazin, P. E. & Tretyakov, Y. D. (2003). *Solid State Sci.* **5**, 1277–1283.
Kharton, V. V., Shaula, A. L., Patrakeev, M. V., Waerenborgh, J. C., Rojas, D. P., Vyshatko, N. P., Tsipis, E. V., Yaremchenko, A. A. & Marques, F. M. B. (2004). *J. Electrochem. Soc.* **151**, A1236–A1246.
León-Reina, L., Losilla, E. R., Martinez-Lara, M., Bruque, S. & Aranda, M. A. G. (2004). *J. Mater. Chem.* **14**, 1142–1149.
León-Reina, L., Losilla, E. R., Martinez-Lara, M., Bruque, S., Llobet, A., Sheptyakov, D. V. & Aranda, M. A. G. (2005). *J. Mater. Chem.* **15**, 2489–2498.
León-Reina, L., Losilla, E. R., Martinez-Lara, M., Martin-Sedeño, M. C., Bruque, S., Nunez, P., Sheptyakov, D. V. & Aranda, M. A. G. (2005). *Chem. Mater.* **17**, 596–600.

León-Reina, L., Martin-Sedeño, M. C., Losilla, E. R., Cabeza, A., Martinez-Lara, M., Bruque, S., Marques, F. M. B., Sheptyakov, D. V. & Aranda, M. A. G. (2003). *Chem. Mater.* **15**, 2099–2108.
León-Reina, L., Porras-Vazquez, J. M., Losilla, E. R. & Aranda, M. A. G. (2006). *Solid State Ion.* **177**, 1307–1315.
Mercier, P. H. J., Le Page, Y., Whitfield, P. S. & Mitchell, L. D. (2006). *J. Appl. Cryst.* **39**, 369–375.
Mercier, P. H. J., Le Page, Y., Whitfield, P. S., Mitchell, L. D., Davidson, I. J. & White, T. J. (2005). *Acta Cryst.* B**61**, 635–655.
Nakayama, S. & Higuchi, M. (2001). *J. Mater. Sci. Lett.* **20**, 913–915.
Nakayama, S., Kageyama, T., Aono, H. & Sakaoka, Y. (1995). *J. Mater. Chem.* **5**, 1801–1805.
Ohnuki, T., Kozai, N., Samadfam, M., Yasuda, R., Yamamoto, S., Narumi, K., Naramoto, H. & Murakami, T. (2004). *Chem. Geol.* **211**, 1–14.
Okudera, H., Masubuchi, Y., Kikkawa, S. & Yoshiasa, A. (2005). *Solid State Ion.* **176**, 1473–1478.
Povarennykh, A. S. (1972). *Crystal Chemical Classification of Minerals*, pp. 541–542. New York/London: Plenum Press.
Rietveld, H. (1969). *J. Appl. Cryst.* **2**, 65–71.
Rodriguez-Carvajal, J. (1990). *FULLPROF*. Version 3.5d. LLB, CEA/Saclay, France.
Sears, V. F. (1993). *International Tables for Crystallography*, edited by A. J. C. Wilson, Vol. C, pp. 383–391. Dordrecht: Kluwer Academic Publishers.
Slater, P. R. & Sansom, J. E. H. (2003). *Solid State Phenom.* **90–91**, 195–200.
Slater, P. R., Sansom, J. E. H. & Tolchard, J. R. (2004). *Chem. Rec.* **4**, 373–384.
Smahi, A., Solhy, A., El Badaoui, H., Amoukal, A., Tikad, A., Maizi, M. & Sebti, S. (2003). *Appl. Catal. Gen.* **250**, 151–159.
Tolchard, J. R., Islam, M. S. & Slater, P. R. (2003). *J. Mater. Chem.* **13**, 1956–1961.
Tolchard, J. R., Sansom, J. E. H., Islam, M. S. & Slater, P. R. (2005). *Dalton Trans.* pp. 1273–1280.
White, T., Ferraris, C., Kim, J. & Madhavi, S. (2005). *Apatite – An Adaptive Framework Structure*, Vol. 57, *Reviews in Mineralogy and Geochemistry*, edited by G. Ferraris & S. Merlino, pp. 307–401. Washington, DC: Mineralogy Society of America.
White, T. J. & ZhiLi, D. (2003). *Acta Cryst.* B**59**, 1–16.